Hindawi
Shock and Vibration
Volume 2019, Article ID 4038657, 14 pages
https://doi.org/10.1155/2019/4038657

Research Article

Vibration Control Performance Analysis and Shake-Table Test of a Pounding Tuned Rotary Mass Damper under the Earthquake

Shujin Li, Lei Sun, and Fan Kong

School of Civil Engineering and Architecture, Wuhan University of Technology, Luoshi Road No. 122, Wuhan 430070, China

Correspondence should be addressed to Fan Kong; kongfan@whut.edu.cn

Received 28 April 2019; Accepted 11 June 2019; Published 1 August 2019

Academic Editor: Marco Tarabini

The voided biaxial concrete slab has been widely used in the engineering field. The slab has become a popular choice for designers and architects looking to reduce slab thickness and overall structure weight recently. Utilizing the empty space in the voided slab and introducing the structural control technology of mass damper into it, a new pounding tuned rotary mass damper (PTRMD) is proposed in this paper. This damper is designed to locate in the prefabricated hollow module to mitigate response of structure subject to disastrous excitations. The damper combines the characteristics of pounding mechanisms (PMDs) and tuned rotary mass dampers (TRMDs). This is achieved by a ball rolling on a curved orbit and a fixed stroke-limiting plate. The structural control performance of the PTRMD is studied numerically and verified experimentally. Specifically, first, the motion equations for a single-degree-of-freedom (SDOF) and multiple-degree-of-freedom (MDOF) system with PTRMDs are derived. Furthermore, numerical results show that the PTRMD provides significant energy dissipation, and thus, is quite effective in reducing the structure response. Besides, the PTRMD generally exhibits better control performance and robustness in terms of vibration suppression compared with the TRMD proposed by the authors before. Finally, a shake-table test is conducted to verify the damping effect of a PTRMD-controlled SDOF system. Pertinent results confirm the effectiveness and robustness of PTRMDs for structural control.

1. Introduction

Structural systems with voided biaxial slabs have been widely used in engineering applications in Europe [1, 2] and China. Schnellenbach-Held and Pfeffer [3], for instance, investigated the structural behavior of a type of biaxial voided slab called BubbleDeck used in Europe. This voided slab consists of a hollow ball made of recycled industrial plastic [3]. BubbleDeck is employed to act as a normal monolithic two-way spanning concrete slab. Other examples of similar hollow modules include U-boot [2]. The main advantages of biaxial voided slabs are that they reduce dead weight and extend the span of structural floors [4]. The most important feature of these hollow modules is their large voided interior space.

In a previous study [5], the authors proposed a new type of damper, namely, the tuned rolling mass damper (TRMD) that takes advantage of the large space in voided modules to avoid the excessive occupation of building space often encountered in pendulum-like tuned mass damper (TMD) applications. However, the study shows the TRMDs have a problem as for TMDs, i.e., they have limited response reduction capacity for seismic control [6–8]. The reason may attribute to that the frequency response function of the linear TMDs is quite narrow compared to the frequency band of seismic response of MDOF systems. Therefore, an introduction of nonlinear mechanism into the linear TMDs may benefit to the controlling effect. In this regard, one may consider the use of the pounding tuned mass damper (PTMD) that combines a traditional TMD and a collision mechanism proposed in a previous study [9]. Specifically, based on a traditional TMD, a PTMD adds buffer made of viscoelastic materials to limit the stroke of the mass [10]. The system acts as a traditional linear TMD without pounding when the stroke is inside of the buffers, whereas it acts as a nonlinear TMD when a larger stroke occurs. This high

degree of nonlinearity is due to the impact between the oscillator and the buffers. In the impact process, mechanical energy is dissipated as heat and noise.

Zhang et al. [9] utilized PTMD for response control of a transmission tower. The performance of the PTMD under earthquake conditions was studied, and the numerical results confirmed that the PTMD was more effective than a TMD. The influence of parameters such as the mass ratio, clearance, seismic intensity, and structural damping ratio was analyzed. Li et al. [11] investigated the performance of a PTMD on a traffic signal pole. The pounding mechanism of the PTMD was verified experimentally, with its performance under conditions of free vibration and resonant excitation exceeding that of a TMD [12–14]. The acceleration response of the control signal under conditions of sine-wave excitation was reduced by 55%, which is an important and significant result. Li et al. [12] applied a PTMD to a subsea jumper to study the robustness of the damper when confronted with detuning effects. It was found that [12] the PTMD performed best when the excitation frequency was slightly lower than the fundamental frequency, which is the optimal frequency. Xue et al. [13] took an offshore platform as an example and reached the same conclusion, i.e., PTMD is more effective and robust than TMD. Previous studies demonstrate that viscoelastic collision mechanisms significantly improve the damping performance and robustness of the traditional TMDs. However, most studies [14–16] investigated impact dampers, be they theoretical or experimental, focusing on the performance of SDOF systems under simple excitation conditions such as sinusoidal loading. Most civil structures, for instance, multistory buildings, experiencing situations such as strong winds or earthquakes, cannot reasonably be approximated as an SDOF system and complex external loading is likely to induce more than just the fundamental mode [16].

In this paper, a novel pounding tuned rotary mass damper (PTRMD) that combines a buffered pounding mechanism to the design of a TRMD is presented. Specifically, first, the equations of motion relating to SDOF/MDOF structure controlled by a PTRMD are derived. Next, the control performance of three different loading conditions for an SDOF system, including free vibration, harmonic excitations, and seismic excitation is investigated. Furthermore, a 6-story structure is used as an illustrative example for control performance of an MDOF systems equipped with PTRMD. PTRMDs of varying frequencies are introduced into this numerical simulation to study the robustness of the system. Finally, experiments involving free vibration and seismic response of PTRMD-controlled SDOF structure are conducted to verify the effectiveness of the proposed control device.

2. Pounding Tuned Rotary Mass Damper System

2.1. Primary Structure. A structure with a voided biaxial reinforced concrete slab is the primary structure to be controlled. The main elements of this slab are prefabricated, hollow, box-like modules (Figure 1) located between the

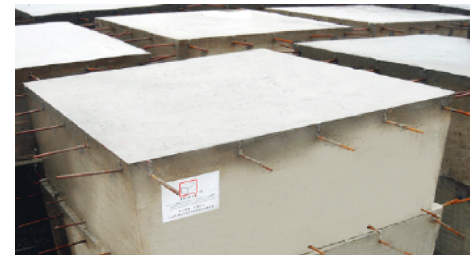

Figure 1: Prefabricated box of hollow floor.

reinforcement grids of the main beams and the ribbed beams. The modules are used as the side formwork site-casting the concrete beams. In this way, only the bottom formworks of the concrete slab are needed, thus saving a considerable mass of the structure. Figure 2 shows a simplified diagram of a hollow floor with a pounding tuned rotary mass damper. The damper consists of a single rectangular hollow box, a ball rolling along an arch path, and two buffering stop plates. Compared to the other TMDs, the proposed PTRMD system does not alter the architectural interior space excessively. Previous studies [13] indicated that an enhanced control effect could be achieved by introducing a flexible buffer zone between a moving damper mass and its boundaries. Stop plates covered with viscoelastic materials are therefore installed in the hollow-floor cavity.

2.2. Models of Mass Dampers. Figures 3(a)–3(c) illustrate a TRMD, pounding mass damper (PMD), and PTRMD model used for a hollow-ribbed floor. The PTRMD consists of two parts, i.e., the TRMD part and the pounding part. The TRMD part, as shown in Figure 3(a) is a hollow module with an arced path supporting a rolling ball. This part absorbs structural mechanical energy by tuning the damper frequency to the fundamental structure frequency and through the friction generated on the mass-path interface. The pounding part is two stroke-limiting plates covered with viscoelastic materials located on both sides of the mass equilibrium position. A pounding/impact mass damper without tunable frequency is shown in Figure 3(b). Once the mass stroke exceeds the allowed clearance, the mass impacts the inner side of the plates, causing mechanical energy to dissipate in the form of heat and noise. In brief, the PTRMD has two energy dissipation mechanisms, one derived from the pounding mechanism and another originated from the tuned mass damper.

2.3. Governing Equation for an SDOF PTRMD Structure. The structure equipped with a PTRMD can be considered as a model with two degrees of freedom for numerical analysis, as shown in Figure 3(c). In this context, one may use Lagrange's equation to derive the equations of the motion of the controlled system, in which the angular motion of the rolling mass is considered to be a small quantity. That is,

$$\frac{d}{dt}\left(\frac{\partial T}{\partial \dot{q}_i}\right) - \frac{\partial T}{\partial q_i} + \frac{\partial V}{\partial q_i} = Q_i^{\mathrm{nc}}, \quad i = 1, 2, \tag{1}$$

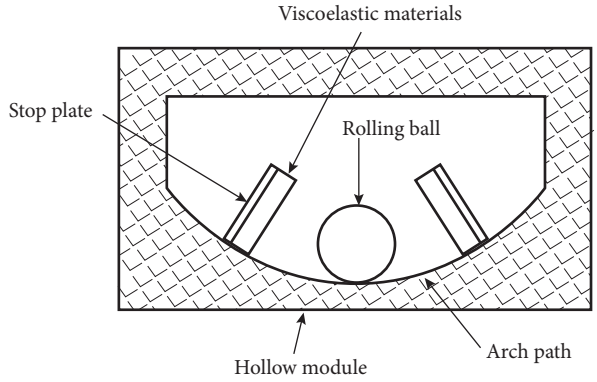

Figure 2: Schematic diagram of PTRMD.

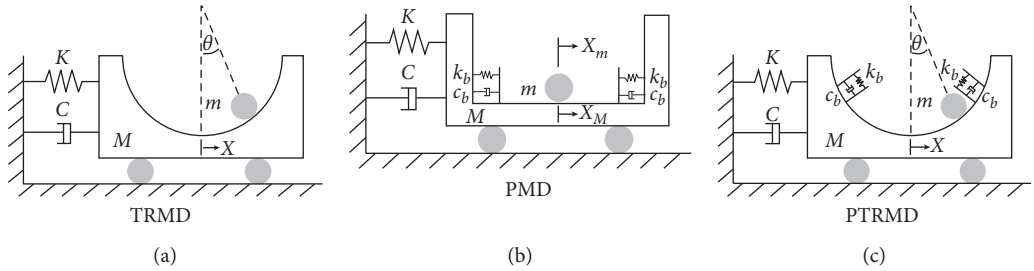

Figure 3: Schematic diagram of the physical model of a (a) TRMD, (b) PMD, and (c) PTRMD.

where T is the kinetic energy of the controlled structure; V is its potential energy; q_i is the i^{th} generalized coordinates; $\dot{q}_i$ is the generalized velocity of the i^{th} coordinate; and Q_i^{nc} is the nonconservative force with respect to q_i.

First, consider the situation when no collision occurs. In this case, the angular displacement of the mass θ satisfies $-\theta_{\text{m}} \le \theta \le \theta_{\text{m}}$, where θ_m is the angular displacement of the oscillator with respect to the center of the arced path when a collision occurs. In this case, the kinetic and potential energy of the controlled structure can be written as follows:

$$T = \frac{1}{2}M\dot{x}^2 + \frac{1}{2}m(\dot{x} + \rho\dot{\theta}\cos\theta)^2 + \frac{1}{2}m(\rho\dot{\theta}\sin\theta)^2 + \frac{1}{5}m(\rho\dot{\theta})^2, \tag{2}$$

$$V = \frac{1}{2}Kx^2 + mg\rho(1 - \cos\theta), \tag{3}$$

where x, $\dot{x}$, and $\ddot{x}$ are the displacement, velocity, and acceleration of the main structure, respectively; M is the mass of the main structure; K is its stiffness; θ, $\dot{\theta}$, and $\ddot{\theta}$ are the angular displacement, angular velocity, and angular acceleration of the oscillator, respectively; m is the mass of the oscillator/ball; ρ is the radius difference between the arced path and the oscillator; and g is the acceleration of gravity.

The nonconservative force Q_i^{nc}, including the external force and the damping force of the structure, can be written as follows:

$$Q_1^{\text{nc}} = f(t) - C\dot{x}, \qquad Q_2^{\text{nc}} = 0, \tag{4}$$

where C is the damping constant of the main structure and $f(t)$ is the external force. Assuming the angular motion of the oscillator θ is very small [5, 6] and combing equations (2)–(4) with equation (1), yield the equation of motion:

$$(M + m)\ddot{x} + m\rho\ddot{\theta} + C\dot{x} + Kx = f(t), \tag{5a}$$

$$\ddot{\theta} + \frac{5\ddot{x}}{7\rho} + \frac{5g\theta}{7\rho} = 0. \tag{5b}$$

Equations (5a) and (5b) can be rewritten in a more compact form:

$$\begin{bmatrix} M+m & m\rho \\ \frac{5}{7\rho} & 1 \end{bmatrix}\begin{Bmatrix} \ddot{x} \\ \ddot{\theta} \end{Bmatrix} + \begin{bmatrix} C & 0 \\ 0 & 0 \end{bmatrix}\begin{Bmatrix} \dot{x} \\ \dot{\theta} \end{Bmatrix} + \begin{bmatrix} K & 0 \\ 0 & \frac{5g}{7\rho} \end{bmatrix}\begin{Bmatrix} x \\ \theta \end{Bmatrix} = \begin{Bmatrix} f(t) \\ 0 \end{Bmatrix}. \tag{6}$$

The left side of equation (5b) shows that the undamped natural frequency of the oscillator depends on the radius difference between the arced path and the oscillator, which can be written as $\omega_{\text{d}} = \sqrt{5g/(7\rho)}$. To obtain an optimum controlled system, the natural frequency of the TRMD needs to match the first modal frequency of the main structure.

Next, consider the situation when a collision occurs. In this case, $\theta \le -\theta_{\text{m}}$ or $\theta \ge \theta_{\text{m}}$, the ball collides with one of the stroke-limiting plates. The potential energy of the controlled structure can be written as follows:

$$V = \frac{1}{2}Kx^2 + mg\rho\left(\cos\theta - \cos\theta_{\mathrm{m}}\right) + \frac{1}{2}k_{\mathrm{b}}\left[\rho\left(\theta - \theta_{\mathrm{m}}\right)\right]^2, \tag{7}$$

where k_{b} is the equivalent contact stiffness for the PTRMD and c_{b} is the equivalent contact damping constant for the PTRMD [17, 18]; In this case, the nonconservative force Q_i^{nc} can be expressed as follows:

$$\begin{aligned} Q_1^{\mathrm{nc}} &= f(t) - c\dot{x}, \\ Q_2^{\mathrm{nc}} &= -c_{\mathrm{b}}\dot{\theta}\rho^2. \end{aligned} \tag{8}$$

Once again, as the angular motion of the oscillator θ is very small, combining equation (2) with equations (7) and (8) gives

$$(M+m)\ddot{x} + m\rho\ddot{\theta} + C\dot{x} + Kx = f(t), \tag{9a}$$

$$\ddot{\alpha} + \frac{5\ddot{x}}{7\rho} + \frac{5c_{\mathrm{b}}\dot{\alpha}}{7m} + \frac{5k_{\mathrm{b}}\alpha}{7m} = 0, \tag{9b}$$

where $\alpha = \theta - \theta_{\mathrm{m}}$. Equations (9a) and (9b) can be cast in a compact form:

$$\begin{bmatrix} M+m & m\rho \\ \dfrac{5}{7\rho} & 1 \end{bmatrix}\begin{Bmatrix} \ddot{x} \\ \ddot{\alpha} \end{Bmatrix} + \begin{bmatrix} C & 0 \\ 0 & \dfrac{5c_{\mathrm{b}}}{7m} \end{bmatrix}\begin{Bmatrix} \dot{x} \\ \dot{\alpha} \end{Bmatrix} + \begin{bmatrix} K & 0 \\ 0 & \dfrac{5k_{\mathrm{b}}}{7m} \end{bmatrix}\begin{Bmatrix} x \\ \alpha \end{Bmatrix} = \begin{Bmatrix} f(t) \\ 0 \end{Bmatrix}. \tag{10}$$

2.4. Governing Equation of an MDOF PTRMD Structure. The equation of motion of a MDOF structure with a PTRMD located at the top floor can be written as follows [12]:

$$\mathbf{M}\ddot{\mathbf{x}}(t) + \mathbf{C}\dot{\mathbf{x}}(t) + \mathbf{K}\mathbf{x}(t) = \mathbf{F}(t) + \mathbf{H}f_{\mathrm{c}}(t), \tag{11}$$

where $\ddot{\mathbf{x}}(t)$, $\dot{\mathbf{x}}(t)$, and $\mathbf{x}(t)$ are the acceleration, velocity, and displacement vectors of the MDOF structure, respectively; Each vector, for example, $\mathbf{x}(t) = [x_1, x_2, \ldots, x_n, \theta]^{\mathrm{T}}$, contains n entries for the n-DOF structure and one entry for the tuned mass; $\mathbf{M}, \mathbf{C}$ and $\mathbf{K}$ are the $(n+1)\times(n+1)$ mass, damping, and stiffness matrices, respectively; $\mathbf{F}(t)$ denotes the vector of the external excitation; $f_{\mathrm{c}}(t)$ is the interaction force between the main structure and the ball, which can be calculated using equation (12) [12, 19–21]. $\mathbf{H} = [\underbrace{0, 0, \ldots, 0}_{n\,\text{times}}, 1]^{\mathrm{T}}$ denotes the location of $f_{\mathrm{c}}(t)$, which can be written as

$$f_{\mathrm{c}}(t) = \begin{cases} -\dfrac{5g}{7\rho}\theta, & |\theta| \le \theta_{\mathrm{m}}\ (\text{no collision}), \\ -\dfrac{5c_{\mathrm{b}}}{7m}\dot{\theta} - \dfrac{5k_{\mathrm{b}}}{7m}\left(\theta - \theta_{\mathrm{m}}\right), & |\theta| > \theta_{\mathrm{m}}\ (\text{collision}). \end{cases} \tag{12}$$

In equation (11), $\mathbf{M}, \mathbf{C}$, and $\mathbf{K}$ are defined as

$$\mathbf{M} = \begin{bmatrix} \mathbf{M}_{\mathrm{s}} + \Gamma\Gamma^{\mathrm{T}}m & \Gamma m\rho \\ \Gamma^{\mathrm{T}}\dfrac{5}{7\rho} & 1 \end{bmatrix}, \quad \mathbf{C} = \begin{bmatrix} \mathbf{C}_{\mathrm{s}} & 0 \\ 0 & 0 \end{bmatrix}, \quad \mathbf{K} = \begin{bmatrix} \mathbf{K}_{\mathrm{s}} & 0 \\ 0 & 0 \end{bmatrix}, \tag{13}$$

where $\mathbf{M}_{\mathrm{s}}, \mathbf{C}_{\mathrm{s}}$, and $\mathbf{K}_{\mathrm{s}}$ are the $n \times n$ mass, damping, and stiffness matrices of the controlled structure, respectively; $\Gamma = [\underbrace{0, 0, \ldots, 0}_{n-1\,\text{times}}, 1]^{\mathrm{T}}$ denotes the location of the damper.

3. Control Performance of an SDOF Structure with PTRMD

A single-degree-of-freedom structure with a PTRMD subjected to three different loading scenarios, free vibration, harmonic excitation, and different intensities of earthquake excitation is considered. The parameters are listed in Table 1, and θ_m was chosen to be 0.13 rad [6, 13]. A PMD shown in Figure 3(b) with the same parameters is employed for comparison, where the stroke length equals to the projection length of the arced path in the PTRMD.

3.1. Free Vibration. In the case of free vibration, an initial displacement of 0.015 m is applied to the structure. Figure 4 shows the dynamic responses of the structure with PMD, with PTRMD, and without control for comparison. The figure shows that the PTRMD mitigates the vibration effectively. For the first 8.7 s, the damping rate with the PTRMD is quite rapid, whereas after 8.7 s, a beat oscillation can be observed in the dynamic response of the structure. One can conclude that the PTRMD is no longer functioning after 8.7 s, indicating that the rolling ball does not impact with the plates anymore. From then on, the system works as a TRMD and dissipates mechanical energy by means of structural damping and the interface friction. Further inspection illustrates that the dynamic response of a structure with a TRMD diminishes with time.

In the case of a PMD (again see Figure 4), the vibration reduction is quite effective. However, it took 5 s for the PMD to reduce the displacement of the main structure to 1 mm while the PTRMD only needed 3.8 s. This implies that the vibration reduction performance of a PTRMD is better than a PMD. Figure 5 shows a comparison of the velocity of the ball rolling in the hollow with the PMD and PTRMD. It is noticeable that the ball's velocity in the PTRMD system is faster than the one in the PMD system from 5.5 s to 8.7 s. Besides, for a PMD, one may conclude that the velocity of the ball at the moment it collides with the stroke-limiting plates depends entirely on the linear velocity of the ball at the end of the previous collision. By contrast, the ball in a PTRMD system located in the curved track can absorb the structural energy, convert it into its own kinetic energy, and

Table 1: Parameters of the PTRMD model.

M	K	C	m	ρ	k_b	c_b
840 kg	58700 N/m	280 N·s/m	16.8 kg	0.1002 m	3000 N/m	50 N·s/m

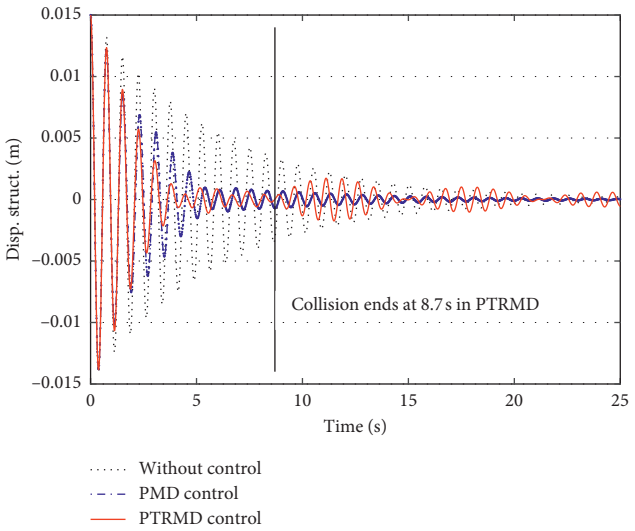

Figure 4: Free decaying displacement of the uncontrolled structure and the controlled structure with PMD and PTRMD.

finally dissipate the energy out. The preceding argument indicates that the energy-consuming capacity of a PTRMD is more efficient, especially at the early phase of the response.

3.2. Harmonic Excitation. For the forced vibrations subject to harmonic excitation, consider first the resonant case, i.e., the excitation frequency equals to the fundamental frequency of the structure. In this case, choose $f(t) = 100 \cdot \sin \omega t$ and $\omega = 8.4$ rad/s. Figure 4 shows a comparison between the responses of the same structure without control, controlled by a PMD, and controlled by the PTRMD. Similar to the situation in Section 3.1, parameters of the stroke-limiting plate (c_b, k_b) in the PMD equal the ones in the PTRMD. Excitation with nonresonant frequency is also investigated from 0 to 15 rad/s [13].

For the resonant case, Figure 6 shows a comparison of the responses to harmonic excitation for the three different scenarios. It can be seen that the PTRMD has the best control performance, although the PMD also reduced the stationary amplitude significantly. Figure 7 shows the response amplitudes of the main structure versus excitation frequencies. From Figure 7, one can conclude that the PTRMDs are more effective than PMDs in the resonant case. When the frequency of the excitation is lower than 8 rad/s or higher than 9 rad/s, both the PTRMD and the PMD are unable to control the vibration effectively.

3.3. Seismic Control Performance. Considering the same structures, uncontrolled or controlled by the PMD and PTRMD, subjected to El Centro and Kobe excitation with a

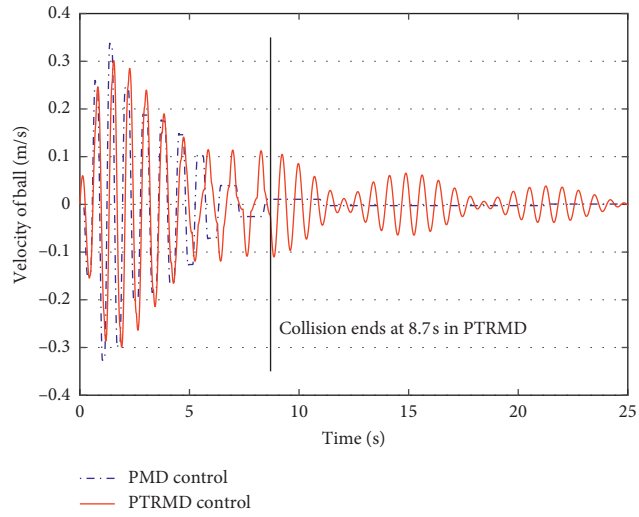

Figure 5: Velocity of the rolling ball in PMD and PTRMD when the structure subject to initial displacement.

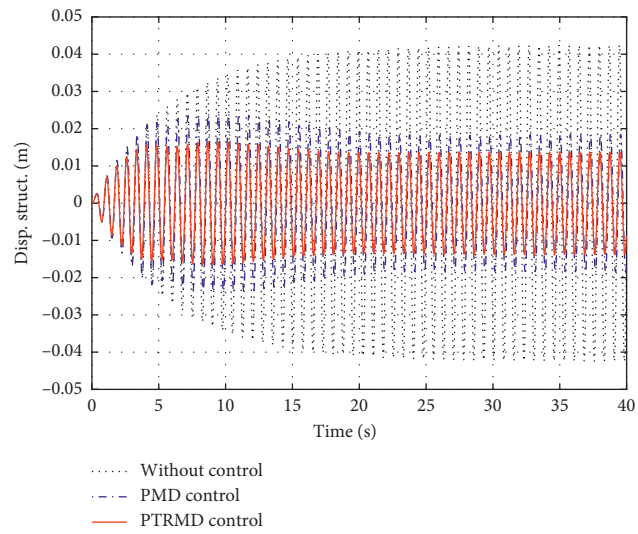

Figure 6: Response of PMD- and PTRMD-controlled structure subject to harmonic excitation.

peak value of 110 cm/s^2, the EL Centro wave (May 18, 1940) has a north-south acceleration peak of 341.7 cm/s^2 and the Kobe wave (January 16, 1995, Kobe, Japan) has a north-south acceleration peak of 821 cm/s^2. Figures 8(a) and 8(b) show response comparisons between the three different control scenarios under two earthquake excitations, respectively. It is seen that although the effectiveness of the PMD and PTRMD systems on peak mitigation is not significant, the responses after the peak are well controlled.

To further investigate the effectiveness of the PTRMD, control efficiency from an energy perspective is examined. Figures 9(a), 9(b), 10(a), and 10(b) show the total amount of energy input from the earthquake excitation (input energy) and the amount of energy dissipated by structural damping and by the PTRMD or PMD. For the uncontrolled structure,

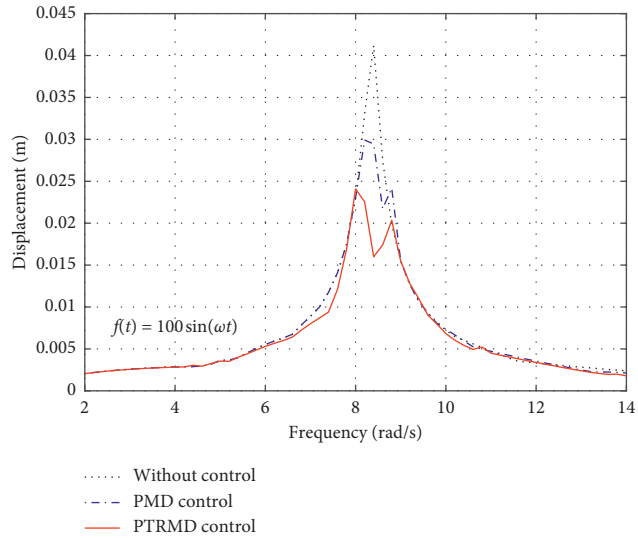

Figure 7: Comparison of the excitation frequency versus response amplitude curves.

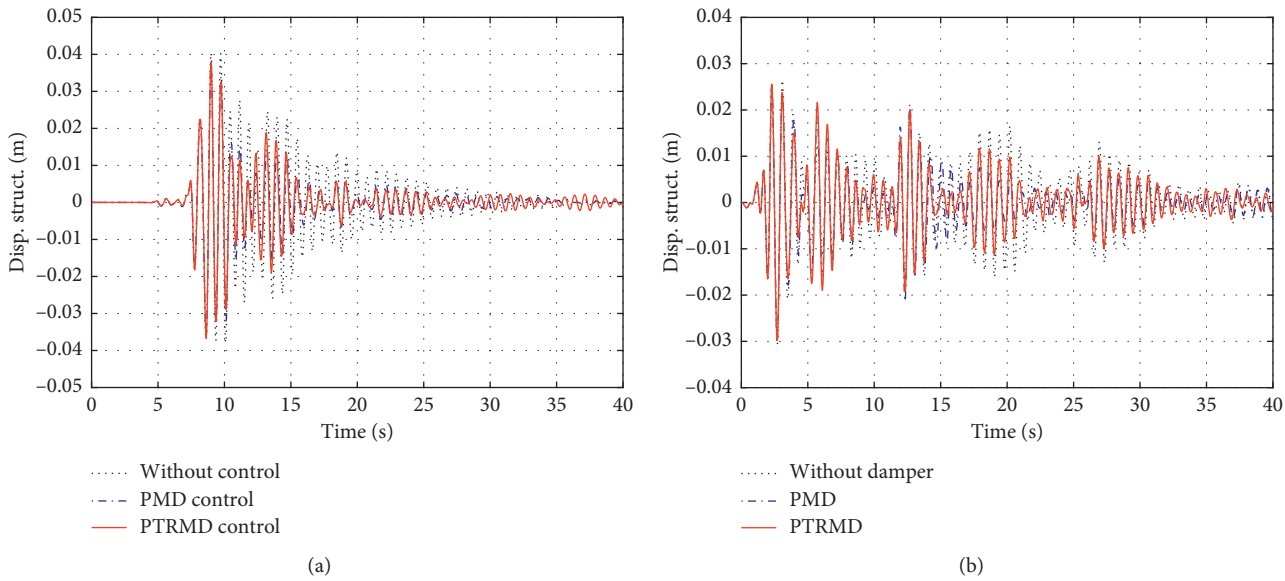

Figure 8: Displacement of the controlled structure under (a) Kobe earthquake and (b) El Centro earthquake.

the sum of the structural strain energy, kinetic energy, and structural viscous damped energy equals the seismic input energy. For the controlled structures, the sum of the three is less than the input energy of the earthquake. The difference between them is the energy dissipated by the external control device. From Figures 10(a) and 10(b), one may conclude that the reason for the PTRMD failing to reduce the peaks can be attributed to the following: at the early stage of the seismic response, neither the angular displacement nor the angular acceleration of the ball oscillator is large enough for producing a collision. With the increment of the structural response and the angular response of the oscillator, effective collisions are finally produced, therefore achieving the designed purpose of energy dissipation.

The control effectiveness of the PTRMD and PMD are compared in Table 2. The energy reduction ratio is 53.0% and 41.8% for the two dampers under the Kobe excitation, respectively. For El Centro excitation case, the energy reduction ratio for the PMD system is 45.7% and increases to 46.8% for the PTRMD system.

4. Seismic Control of an MDOF Structure with PTRMD

Consider a six-floor structure with a lumped-mass model. The lumped masses are assumed to be the same at each floor, i.e., 16.315 t. The stiffness and damping coefficients of each story reduce from the top floor to the ground floor. Instead of assuming a value for the pounding stiffness and the pounding damping, they can be obtained from a linear viscoelastic pounding model [22–25].

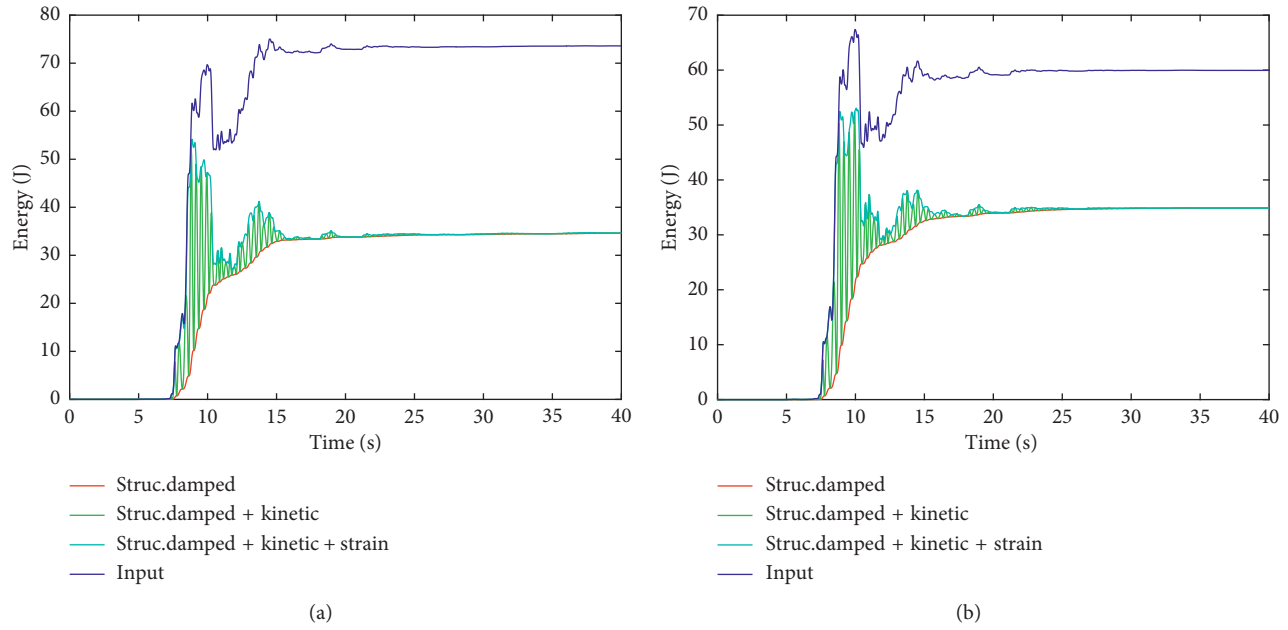

Figure 9: Input and dissipated energy of the controlled structure under Kobe earthquake with a (a) PTRMD and (b) PMD.

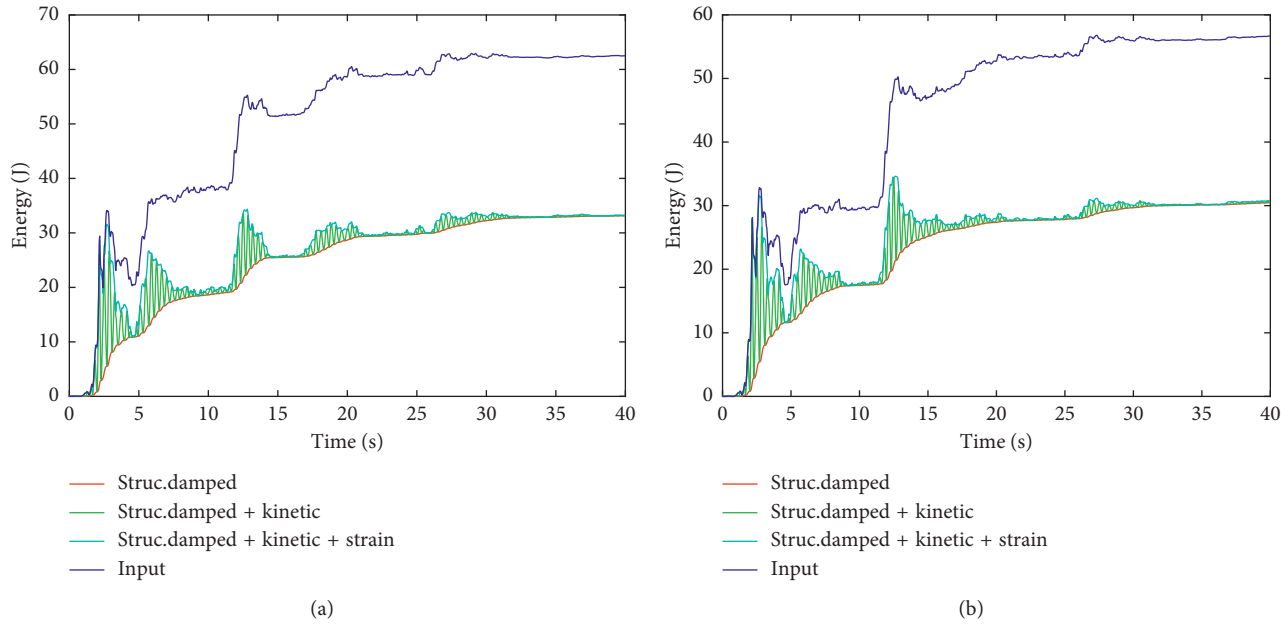

Figure 10: Input and dissipated energy of the controlled structure under El Centro earthquake with a (a) PTRMD and (b) PMD.

Table 2: Comparison of control performance between PTRMD and PMD under earthquake excitation.

Earthquake wave	Damper	D_0 (m)	D_{ctrl} (m)	E_I (J)	E_P (J)	η_E (%)
Kobe wave	PTRMD	0.0404	0.0378	73.5	39.0	53.0
	PMD		0.0373	60.0	25.1	41.8
El centro wave	PTRMD	0.0307	0.0297	38.9	18.2	46.8
	PMD		0.0298	38.6	17.6	45.7

D_{ctrl} and D_0 = displacement responses of the main structure with and without damper. $\eta_E = E_P/E_I$. η_E = energy reduction ratios; E_I = input energy; E_P = energy dissipation of damper.

$$\xi = \frac{-\ln e}{\sqrt{\pi^2 + (\ln e)^2}}, \tag{14}$$

$$k_b = \frac{m}{(1+\lambda)T_c^2}\left[\pi^2 + (\ln e)^2\right],$$
$$c_b = \frac{2m\ln e}{(1+\lambda)T_c}, \tag{15}$$

where ξ is the damping ratio of the pounding boundary; λ is the mass ratio defined as the oscillator mass to the floor mass where the damper installed; and e is the restitutive coefficient

defined as the ratio of the prepounding velocity to the postpounding velocity. Generally, the restitutive coefficient should be measured to determine k_b and c_b. Alternatively, in this numerical example, one may adopt a value of pounding damping coefficient ξ suggested by other studies and obtain the restitutive coefficient e by using equation (14). Assuming $\xi = 0.1$ leads to $k_b = 42.7\,\text{kN/m}^2$ and $c_b = 808\,\text{N·s/m}$ [26]. Other parameters of the PTRMD-controlled MDOF structure are listed in Table 3. In this case, the mass ratio of the oscillator to the first model mass is 0.5%.

The following cases illustrate the control performance of the PTRMD in reducing the MDOF structural response:

Case 1: free vibration. This case investigates the free decaying response of the controlled MDOF structure with initial nonzero displacement. The frequency of the PTRMD is tuned to the first modal frequency to attain an optimal effect.

Case 2: forced vibration. This case investigates the forced harmonic response of the controlled MDOF structure subject to a sinusoidal excitation $F = 2000 \sin(\omega_1 \cdot t)$ at the top floor and $\omega_1 = 1$ Hz.

Case 3: robustness analysis. This case investigates the robustness of the PTRMD with three different detuned frequencies (0.83, 0.98, and 1.13 Hz).

4.1. Free Vibration. The stroke-limiting angle imposed by the pounding mechanism may have a significant influence on the control effect. Figure 11 shows the displacement root mean square (RMS) of the top story with an initial displacement 0.015 m. One can observe that the RMS decreases rapidly as increasing θ_m until $\theta_m = 0.10$ rad; after this, the RMS increases rapidly as increasing θ_m and finally reaches a stationary value. The preceding results could be anticipated since an excessively small clearance ($2\theta_m$) between the pounding boundaries may lead to ineffective collisions increasing, whereas a large clearance may deactivate the pounding mechanism. Therefore, the optimal pounding angle $\theta_m = 0.10$ rad is adopted in this case.

In Figures 12(a) and 13, the dynamic responses of the structure without control, with a TRMD, and with a PTRMD are compared. It can be seen that a PTRMD provides distinct advantages regarding the displacement and acceleration reduction when compared to a TRMD with the same parameters. Specifically, both the TRMD and PTRMD have limited control effect at the beginning phase of the response. After that, the displacement and acceleration of the structure with the PTRMD are significantly reduced. On the contrary, because oscillator-path friction is assumed to be zero, even though a TRMD can absorb energy from the structure quite fast, it cannot dissipate the absorbed energy through an effective damping mechanism. Again, the TRMD absorbed energy transfers to the structure and finally, makes the structure response exhibiting the so-called beat behavior. According to the authors' previous studies, the amplitude of the beats may be smaller but still exists if oscillator-path friction is considered. As for the PTRMD, although the response mitigation rate is slower than the TRMD, no beat behavior is observed in the response. The rotation angle of the oscillator, shown in Figure 12(b), does not exceed the limitation of the small quantity assumption, which is often regarded as 0.3 rad (or about ca. 20°). The rotation angle of the oscillator shows that it is reasonable to use the small quantity assumptions for a linearized equation of motion.

4.2. The Forced Vibration Case. Using a similar method as in Section 3.1, one can determine the value of the pounding angle θ_m to be 0.21 rad. Figures 14 and 15 display the top story responses of the structure with and without a PTRMD when the excitation is a sinusoidal wave. Compared to the displacement of the TRMD, whose peak value at the top floor decreased from 0.08 m to 0.06 m, the displacement for the PTRMD is much smaller, at 0.02 m. A similar conclusion is visible in the acceleration response. In this situation, the PTRMD performed better because the pounding mechanism provides an additional control mechanism.

Figure 16 shows the control effect of the TRMD and PTRMD in the frequency domain, where the horizontal axis denotes the frequencies of harmonic excitations and the vertical stands for the response amplitude at the stationary stage. It is seen that the PTRMD performed better performance over a wide frequency range. Although at a specific frequency interval, for example, at 0.98 Hz, the displacement of the structure with the TRMD is smaller than it is with the PTRMD, and the PTRMD displayed better control for the ranges 0.9 to 0.96 Hz and 0.99 to 1.1 Hz.

4.3. The PTRMD with Detuned Frequencies. The robustness of the PTRMD and TRMD can be investigated by detuning their natural frequencies. Both free vibration and forced vibration are considered.

Figures 17 and 18 show the free vibration of the structure with differently tuned TRMDs and PTRMDs. The optimally tuned PTRMD (i.e., at 0.96 Hz) decreases the RMS of the displacement by 44.2%. However, detuned PTRMDs exhibit different performance. Specifically, the response RMS reduction ratio of the structure with a 1.10 Hz PTRMD is 41.9% and with a 0.82 Hz PTRMD it is only 9.3%. Contrarily, the optimally tuned nonfriction TRMD reduced the RMS of the displacement response by 3.17%. Figure 19 further illustrates the relationship between the vibration reduction ratio and the detuning ratio. The preceding results imply that a PTRMD outperforms a nonfriction or low-friction TRMD for vibration control.

Figures 20 and 21 show the response of the structure when subjected to sinusoidal excitation with the same frequency as in Section 4.2. Consider PTRMDs with three frequencies, including optimally tuned at frequency 1.0 Hz and two detuned frequencies at 1.15 Hz (+15%) and 0.85 Hz (−15%). For the optimally tuned frequency, the peak displacement is reduced by 71.3%, whereas for ±15% detuned frequencies, it is reduced by 57.5% and 67.1%, respectively. It can be concluded that the detuned frequencies have a limited impact on the performance of a PTRMD when the excitation is a sinusoidal wave. It can also be seen from Figure 22 that the vibration control performance of the PTRMD deteriorated less than that of the TRMD when the dampers are detuned.

Table 3: Model parameters of a PTRMD-controlled MDOF structure.

First mode mass M_s (kg)	First mode stiffness K_s (kN/m)	First mode frequency f (Hz)	Ball mass m (kg)	Mass ratio $(m/M_6)\,\lambda$	Radius of ball r (m)	Radius of arc track R (m)
7.9×10^4	3.12×10^6	1	395.3	0.0242	0.23	0.407

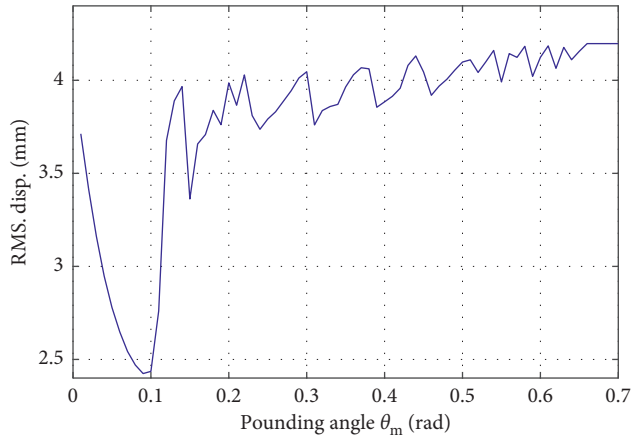

Figure 11: Relation of the structural displacement RMS and pounding angle.

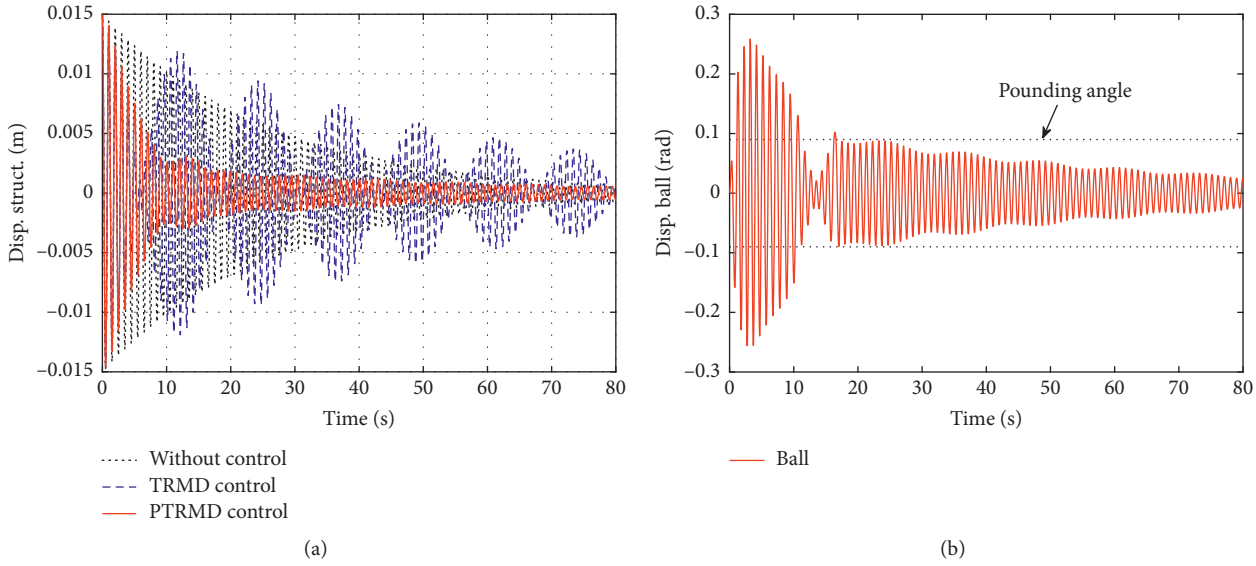

Figure 12: Displacement response of (a) the uncontrolled or TRMD-/PTRMD-controlled structure and (b) the oscillator when the structure subject to an initial displacement.

5. Experimental Verification

5.1. Experimental Setup. Experiments were conducted to investigate the effectiveness of the PTRMD and verify the numerical results. An experimental structure, illustrated in Figure 23, was built to simulate an SDOF linear oscillator. The test model consisted of two sets of $400 \times 100 \times 1$ mm flexible columns made of steel strips and a $300 \times 100 \times 10$ mm beam made of aluminum alloy. In order to fix the model with the shaking table, a $300 \times 100 \times 10$ mm aluminum alloy bottom plate was made. The columns were bolted rigidly to the beam and the base such that the ends were rotationally fixed. The base was fixed to a unidirectional shake table (Shake Table 2, Quanser) that was driven by an electrodynamic shaker to produce base excitation. Dynamic tests show that the frequency of the primary structure is $f_n = 2.27$ Hz and the damping ratio is $\xi = 0.13$.

Figure 24 is a photo of the PTRMD device. Two steel stop plates were fixed on the curved orbit to act as stroke-limiting stops for the freely moving impact mass. The curved track was made of an aluminum alloy plate. The side baffles were made from acrylic-based resins that allowed the ball to roll in the direction of the structural vibration. The parameters of the PTRMD are listed in Table 4.

Experiments were performed to cover two cases. First of all, a free-vibration experiment was carried out by applying

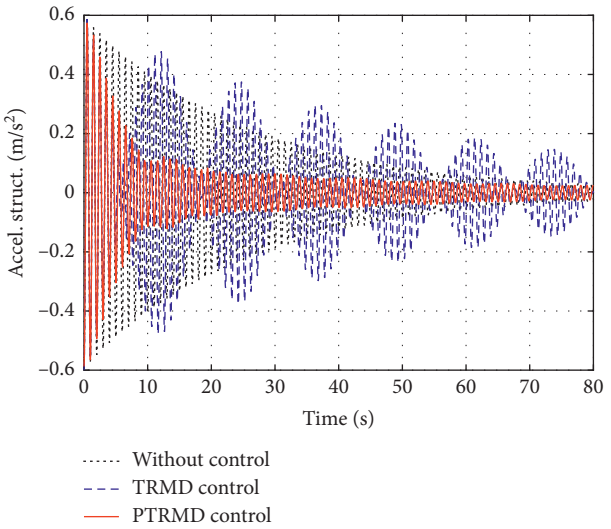

Figure 13: Acceleration response of the structure under free vibration.

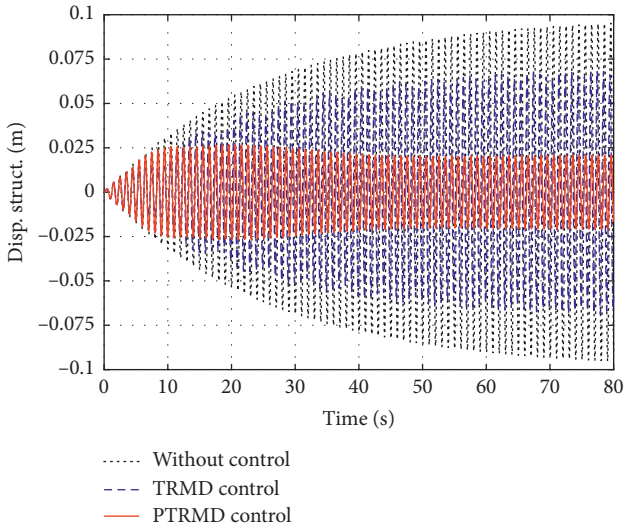

Figure 14: Displacement response of the structure under sinusoidal excitation.

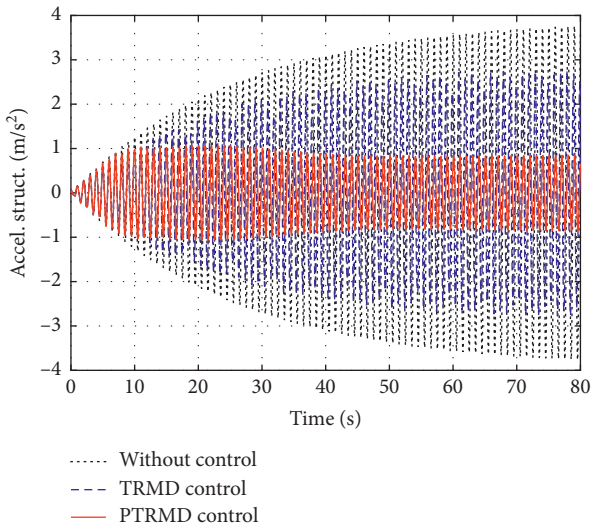

Figure 15: Acceleration response of the structure under sinusoidal excitation.

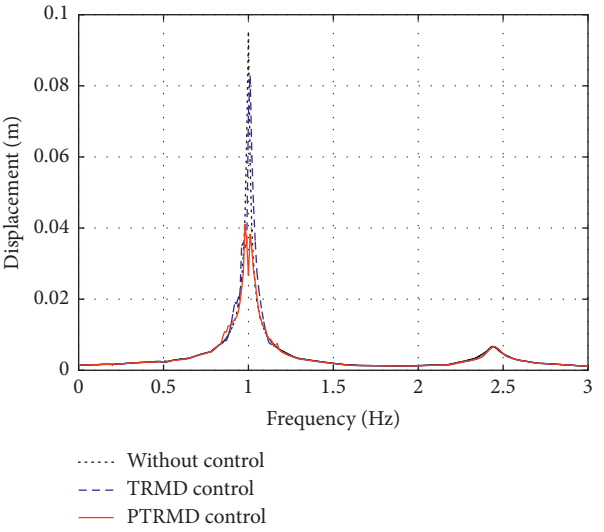

Figure 16: Response of the structure subjected to excitation of varied frequencies.

an initial displacement to the structure and then releasing it. Then, the shaking table tests with different earthquake excitations were conducted.

5.2. Experimental Results. The responses of the PTRMD-controlled structure are compared to the responses of the uncontrolled structure to verify the effectiveness of the PTRMD model. Figure 25 relates to the free vibration scenario. As can be seen, at the beginning of the response, the displacement mitigation performance of the damper is rather limited. As time goes on, the damper exhibits significant performance improvement. The preceding observation is reasonable since effective collision cannot be established until several cycles of oscillation. Specifically, the displacement amplitude of the controlled structure only reached 3 mm, whereas for the uncontrolled structure, it reached 12.6 mm after 10 s. Note also that the wave shape of the controlled response obtained by the experiment is consistent with the one shown in Figure 12(a) qualitatively, demonstrating the effectiveness of the proposed damper.

To quantify the vibration control performance, one can define the response reduction ratio as

$$\beta_t = \frac{D_{un} - D_c}{D_{un}} \times 100\%, \tag{16}$$

where D_c and D_{un} are the displacement envelope of the structure calculated by $D(t) = \sqrt{x^2 + (\dot{x}/\omega_d)^2}$ at a certain time instant with and without the PTRMD, where ω_d is the damped natural frequency. In this numerical simulation, because no flexible viscoelastic material is attached on the stroke-limiting plate, the contact stiffness k_b is set to be 1×10^9 and the constitutive coefficient is 0.01.

Table 5 shows the response reduction ratio of experimental test and of the numerical simulation for controlled

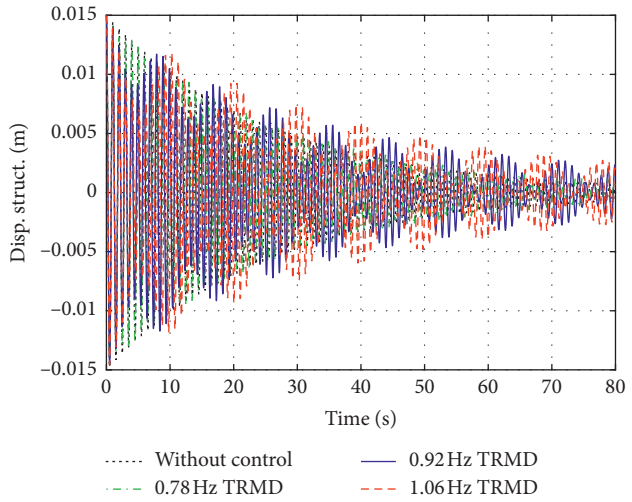

Figure 17: Response of the structure controlled by TRMD with different frequencies for free vibration.

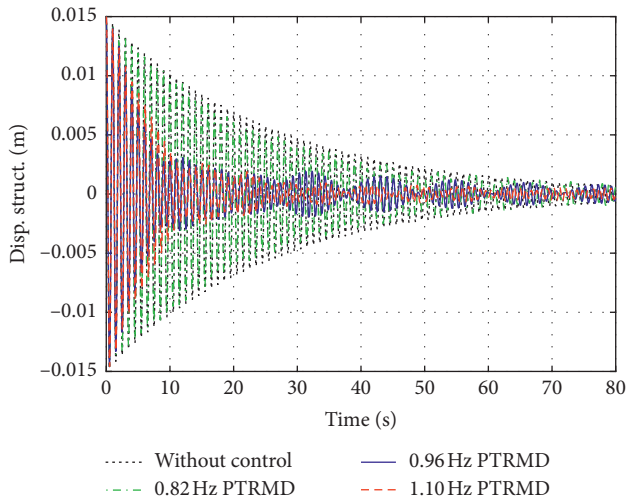

Figure 18: Response of the structure controlled by PTRMD with different frequencies for free vibration.

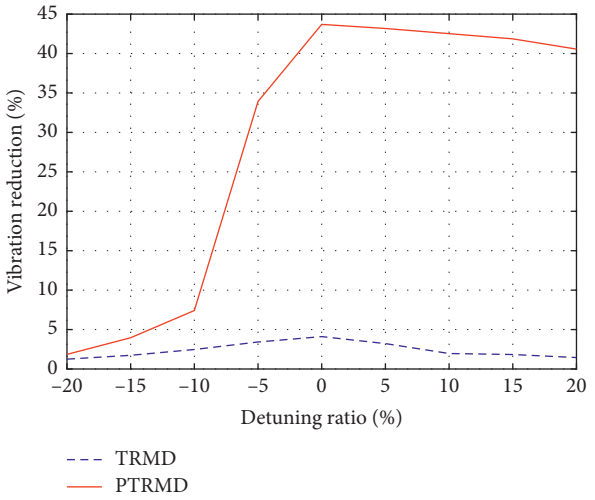

Figure 19: Reduction ratio of the TRMD and PTRMD with different frequencies.

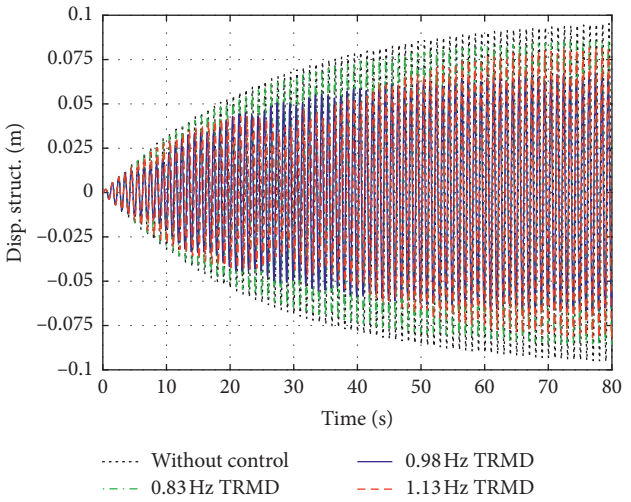

Figure 20: Response of structure controlled by TRMD with different frequencies for forced vibration.

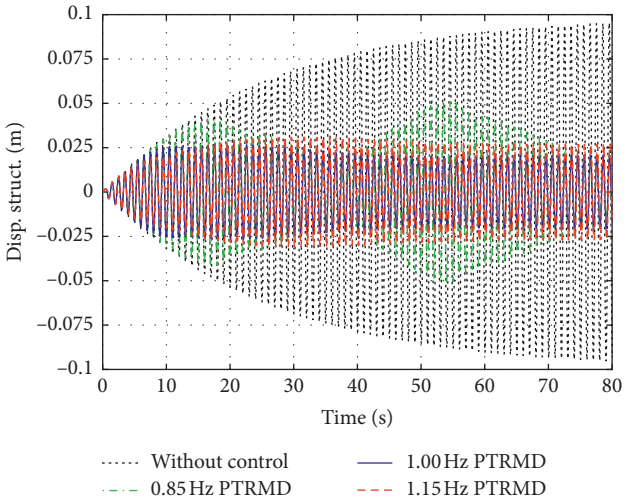

Figure 21: Response of structure controlled by PTRMD with different frequencies for forced vibration.

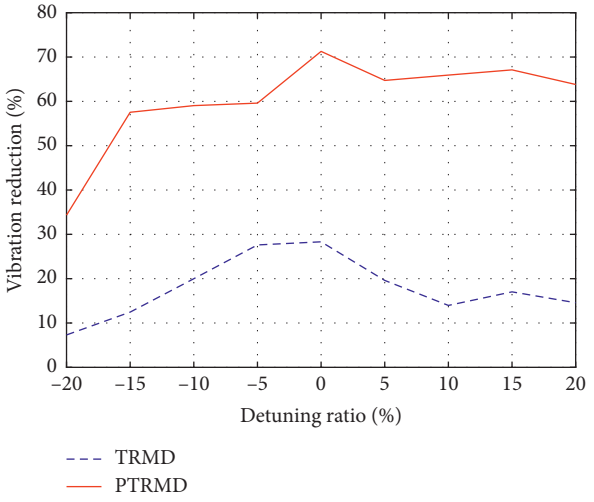

Figure 22: Reduction ratio of TRMD and PTRMD.

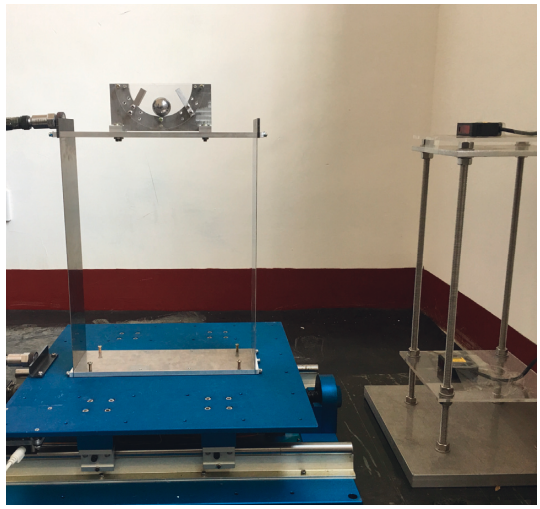

Figure 23: Photograph of the test structure.

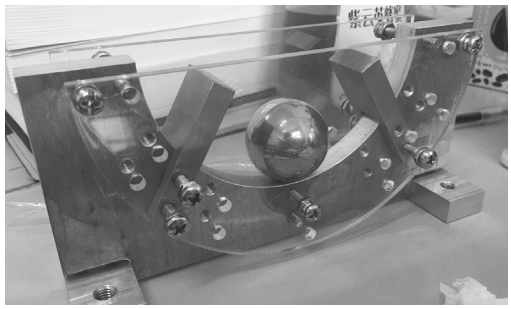

Figure 24: Experiment model of PTRMD.

Table 4: Parameters of PTRMD in test.

Radius of arc track R (mm)	Radius of ball r (mm)	Ball mass m (g)	Radius difference ρ (mm)	D (mm)
50	15	120	34.5	68

where D is the arc clearance between two stops.

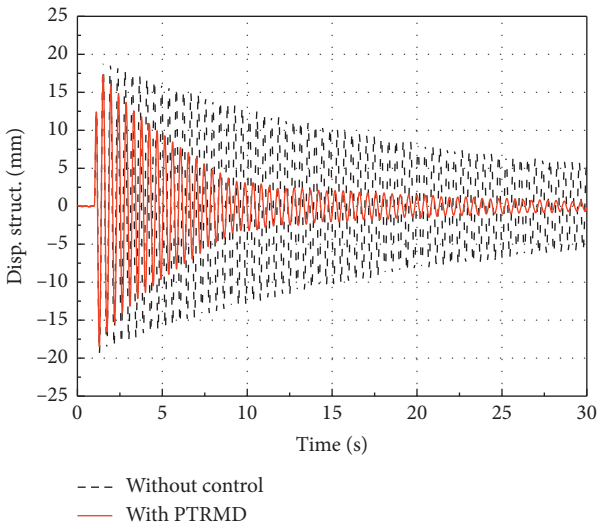

Figure 25: Displacement time history of dynamic response in free vibration.

structure at a different time instant. The experiment data shows that the PTRMD provided a satisfactory response control effect. Besides, the results given by the numerical simulations show reasonable agreement compared to the experimental data. The difference between the experimental and numerical results may attribute to the error in model fabrication, excitation generating of the shaking table, and parameters (for example, k_b, c_b, and e) identification.

Figures 26(a) and 26(b) show a comparison between the response of the primary structure with and without the PTRMD for a Cape Mendocino (April 25, 1992, and north-south) earthquake as an input. It can be seen that the displacement and acceleration of the controlled structure are greatly mitigated, especially after the 5^{th} sec. The controlled response of the model structure subject to El Centro earthquake excitation exhibits similar behavior, which is not shown here. The results measured from the experimental test for Cape Mendocino and El Centro waves are listed in Tables 6 and 7, demonstrating the vibration control effectiveness of the PTRMD.

Table 5: Damping effect of the structure with PTRMD at 10 s, 20 s, and 30 s.

		$D\|_{t=10}$ (mm)	$\beta\|_{t=10}$	$D\|_{t=20}$ (mm)	$\beta\|_{t=20}$	$D\|_{t=30}$ (mm)	$\beta\|_{t=30}$
Experimental results	Uncontrolled	12.62	73.5%	8.56	80.6%	5.26	87.1%
	Controlled	3.34		1.63		0.68	
Numerical results	Uncontrolled	11.41	57.06%	7.01	61.66%	4.90	70.23%
	Controlled	4.90		2.69		1.46	

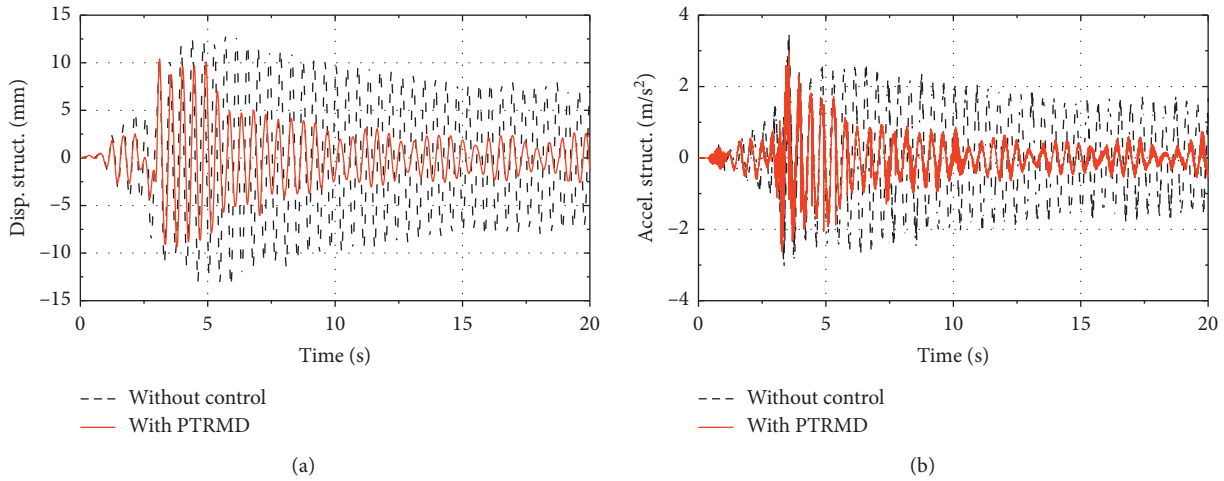

Figure 26: Time history of dynamic response under Cape Mendocino excitation. (a) Displacement. (b) Acceleration.

Table 6: Dynamic responses of the main structure under Cape Mendocino excitation.

Cases	Max. displ. ampl. (mm)	Displ. RMS (mm)	Max. acc. ampl. (m/s^2)	Acc. RMS (m/s^2)
Uncontrolled	13.52	6.44	3.49	1.25
Controlled	10.41	2.95	2.94	0.53
Redn. ratio (%)	23.00	54.19	15.76	57.60

Table 7: Dynamic responses of the main structure under El Centro excitation.

Cases	Max. displ. ampl. (mm)	Displ. RMS (mm)	Max. acc. ampl. (m/s^2)	Acc. RMS (m/s^2)
Uncontrolled	13.47	5.21	3.26	0.99
Controlled	9.98	2.56	2.45	0.45
Redn. ratio (%)	25.91	50.86	24.85	54.55

6. Concluding Remarks

A novel pounding tuned rotary mass damper (PTRMD) exclusively used for the voided biaxial slabs has been introduced in this paper. The proposed damper has been developed by introducing the nonlinear pounding mechanism to the tuned rotary mass damper (TRMD) proposed by the authors in previous studies. Numerical analysis has been used to investigate the control performance of the proposed PTRMD in reducing structural response. Both single-degree-of-freedom (SDOF) and multiple-degree-of-freedom (MDOF) lumped-mass models have been used for this purpose. In the numerical analysis, specifically, the equation of motion of the controlled structure has been established using Lagrange's equation, while the pounding mechanism has been described using a parallel connection of a linear dashpot and a spring (Kelvin model). The PTRMD control performance has been studied quantitatively in different cases including free vibration and forced vibration with sinusoidal excitation and seismic excitation. An experimental study has been carried out to validate PTRMD control performance obtained by numerical analysis. According to the numerical simulation and experimental study, one may draw the following conclusions:

(1) PTRMD outperforms the pounding mass damper (PMD) in reducing the response of an SDOF system in the case of free vibration and sinusoidal excitation. PTRMD exhibits comparably better performance in mitigating response of an SDOF system subject to earthquake excitations.

(2) PTRMD cannot effectively reduce the response amplitude at the early stage when the structure is subject to earthquake excitation. The control performance becomes significant after the pounding mechanism is completely activated.

(3) PTRMD with optimal pounding angle performs better than the TRMD in the case of reducing MDOF system response in the cases of free vibration and forced vibration with sinusoidal excitation. The PTRMD has exhibited improved robustness compared with the TRMD when the frequency of the damper is detuned.

(4) The shaking table experiment results agree reasonably with the numerical ones, validating the effectiveness of the proposed PTRMD.

Data Availability

The numerical simulation and other data used to support the findings of this study are available from the corresponding author upon request.

Conflicts of Interest

The authors declare that there are no conflicts of interest regarding the publication of this paper.

Acknowledgments

This work was supported financially by the National Natural Science Foundation of China (NSFC) (Grant no. 51678464).

References

[1] T. Lai, *Structural Behavior of BubbleDeck® Slabs and Their Application to Lightweight Bridge Decks*, Massachusetts Institute of Technology, Cambridge, MA, USA, 2010.

[2] A. Churakov, "Biaxial hollow slab with innovative types of voids," *Construction of Unique Buildings ad Structures*, vol. 6, no. 21, pp. 70–88, 2014.

[3] M. Schnellenbach-Held and K. Pfeffer, "Punching behavior of biaxial hollow slabs," *Cement and Concrete Composites*, vol. 24, no. 6, pp. 551–556, 2002.

[4] W. B. Ali and G. S. Urgessa, "Structural capacities of spherically voided biaxial slab (SVBS)," in *Proceedings of the Structures Congress 2014*, pp. 785–796, Boston, MA, USA, April 2014.

[5] S. Li, L. Fu, and F. Kong, "Seismic response reduction of structures equipped with a voided biaxial slab-based tuned rolling mass damper," *Shock and Vibration*, vol. 2015, Article ID 760394, 15 pages, 2015.

[6] S. J. Li, J. X. Wang, L. Sun, and F. Kong, "Parameter optimization of new energy dissipation device based on hollow floor slab," *Journal of Architecture & Civil Engineering*, vol. 34, no. 2, pp. 10–17, 2017, in Chinese.

[7] C.-M. Chang, S. Shia, and Y.-A. Lai, "Seismic design of passive tuned mass damper parameters using active control algorithm," *Journal of Sound and Vibration*, vol. 426, pp. 150–165, 2018.

[8] G. Li, L. Li, and P. Zhu, "Galloping control for iced conductors using tuned mass dampers with fixed time-delayed feedback," *Shock and Vibration*, vol. 2019, Article ID 4823457, 9 pages, 2019.

[9] P. Zhang, G. Song, H.-N. Li, and Y. X. Lin, "Seismic control of power transmission tower using pounding TMD," *Journal of Engineering Mechanics*, vol. 139, no. 10, pp. 1395–1406, 2013.

[10] L. Zheng, K. Li, Y. Ouyang, and J. Shan, "Performance-based optimal design of tuned impact damper for seismically excited nonlinear building," *Engineering Structures*, vol. 160, pp. 314–327, 2018.

[11] L. Li, G. Song, M. Singla, and Y.-L. Mo, "Vibration control of a traffic signal pole using a pounding tuned mass damper with viscoelastic materials (II): experimental verification," *Journal of Vibration and Control*, vol. 21, no. 4, pp. 670–675, 2015.

[12] H. Li, P. Zhang, G. Song, D. Patil, and Y. Mo, "Robustness study of the pounding tuned mass damper for vibration control of subsea jumpers," *Smart Materials and Structures*, vol. 24, no. 9, article 095001, 2015.

[13] Q. Xue, J. Zhang, J. He, and C. Zhang, "Control performance and robustness of pounding tuned mass damper for vibration reduction in SDOF structure," *Shock and Vibration*, vol. 2016, Article ID 8021690, 15 pages, 2016.

[14] J. Chen and R. Yang, "Vibration control of tuned rolling-ball damper in wind turbines," *Journal of Tongji University*, vol. 41, no. 8, pp. 1145–1150, 2013, in Chinese.

[15] C. Bapat and S. Sankar, "Single unit impact damper in free and forced vibration," *Journal of Sound and Vibration*, vol. 99, no. 1, pp. 85–94, 1985.

[16] L. Zuo and S. A. Nayfeh, "Minimax optimization of multi-degree-of-freedom tuned-mass dampers," *Journal of Sound and Vibration*, vol. 272, no. 3–5, pp. 893–908, 2004.

[17] K. Li and A. P. Darby, "Modelling a buffered impact damper system using a spring-damper model of impact," *Structural Control & Health Monitoring*, vol. 16, no. 3, pp. 287–302, 2009.

[18] Q. Xue, J. Zhang, J. He, C. Zhang, and G. Zou, "Seismic control performance for pounding tuned massed damper based on viscoelastic pounding force analytical method," *Journal of Sound and Vibration*, vol. 411, pp. 362–377, 2017.

[19] R. Jankowski, "Pounding force response spectrum under earthquake excitation," *Engineering Structures*, vol. 28, no. 8, pp. 1149–1161, 2006.

[20] G. F. D. S. Rebouças, I. F. Santos, and J. J. Thomsen, "Validation of vibro-impact force models by numerical simulation, perturbation methods and experiments," *Journal of Sound and Vibration*, vol. 413, pp. 291–307, 2018.

[21] L. Gordillo, T.-P. Sun, and X. Cheng, "Dynamics of drop impact on solid surfaces: evolution of impact force and self-similar spreading," *Journal of Fluid Mechanics*, vol. 840, pp. 190–214, 2018.

[22] W. Wang, X. Wang, X. Hua, G. Song, and Z. Chen, "Vibration control of vortex-induced vibrations of a bridge deck by a single-side pounding tuned mass damper," *Engineering Structures*, vol. 173, pp. 61–75, 2018.

[23] Y. Zuo, G. Sun, and H. Li, "Response analysis of curved bridge with unseating failure control system under near-fault ground motions," *IOP Conference Series: Earth & Environmental Science*, vol. 108, article 022065, 2018.

[24] E. A. Mavronicola, P. C. Polycarpou, and P. Komodromos, "Spatial seismic modeling of base-isolated buildings pounding against moat walls: effects of ground motion directionality and mass eccentricity," *Earthquake Engineering & Structural Dynamics*, vol. 46, no. 7, pp. 1161–1179, 2017.

[25] A. Guo, Y. Shen, J. Bai, and H. Li, "Application of the endurance time method to the seismic analysis and evaluation of highway bridges considering pounding effects," *Engineering Structures*, vol. 131, pp. 220–230, 2017.

[26] W. Wang, X. Hua, X. Wang, Z. Chen, and G. Song, "Optimum design of a novel pounding tuned mass damper under harmonic excitation," *Smart Material Structures*, vol. 26, no. 5, article 055024, 2017.